Micromorphology of a debris flow deposit: evidence of basal shearing, hydrofracturing, liquefaction and rotational deformation during emplacement

Emrys Phillips

British Geological Survey, Murchison House, West Mains Road, Edinburgh EH9 3LA, Scotland

Telephone: 0131-667-1000. Fax: 0131-668-2683. e-mail: erp@bgs.ac.uk

Abstract

Micromorphological analysis has been applied to a very coarse debris flow deposit and associated sand-dominated glaciofluvial sediments exposed in Westend Wood Quarry, Carstairs, Central Scotland. The microstructures present (folds, faults, plasmic fabrics) within this diamicton and underlying predominantly sandy sediments are interpreted in terms of sedimentary processes active during emplacement of the debris flow. These processes include the formation of a basal shear zone, the deformation and mixing of fine-grained sediments incorporated into the base of overriding debris flow. Features associated with liquefaction, sediment remobilisation and water escape are also present and developed in response to increasing overburden pressure during debris flow emplacement. These microstructures have also been recorded elsewhere within subglacial diamictons, and an evaluation is made between microstructures in palaeo debris flow deposits and those found in modern debris flows.

1. Introduction

Microtextures observed in thin section are increasingly being used to determine sediment genesis (van der Meer 1987; van der Meer & Laban 1990; Seret 1993; Harris 1998; Carr *et al*. 2000; Lachniet *et al*. 2001), unravel complex deformation histories (Phillips & Auton 2000; Menzies 2000; van der Wateren *et al*. 2000) and to elucidate subglacial processes (Menzies & Maltman 1992; van der Meer 1993, 1997; Menzies *et al*. 1997; Menzies 1998; Khatwa & Tulaczyk 2001; Hart & Rose 2001). These studies have, however, largely concentrated upon recognition and classification

of the microstructures present within subglacial diamictons (van der Meer 1993, 1997; Menzies 1998). More recently, Lachniet *et al*. (1999) and Lachniet *et al*. (2001) have examined the range of microstructures developed within debris flow deposits, where sediment released from ablating debris-rich ice is remobilised and deposited under the influence of gravity. During remobilisation and consequent deposition, features present in the source sediment may be overprinted, while debris flow-related structures are developed and preserved (Lawson 1982).

Lawson (1982) and Lachniet *et al*. (1999) recognised four different types of debris flow formed within a modern ice-proximal environment: Type 1 flows which have a water content of between 8 to 14% by weight, are lobate in shape and composed of a cohesive mass flowing over a few centimetres thick basal shear zone; Type 2 flows which have a water content of 14-19%, are commonly channelised, and move as a cohesive mass over basal and lateral shear zones; Type 3 flows have a water content of 18-25%, are channelised, and flow by differential shear throughout; Type 4 flows contain greater than 25% water, may be liquefied, and transport occurs by laminar flow with shear throughout. Laminar flow also dominates transport within the basal shear zones of Type 1 and 2 flows (Lachniet *et al*. 1999). The transport mechanism in all the types of flows is a continuum between a thin basal shear zone supporting a cohesive mass of dry flows, and laminar flow with differential shear occurring throughout the body of wet sediment flows (Lawson 1982). Consequently, debris flow deposits may contain microstructures inherited from the source material, as well as those formed by sediment transport, deposition and/or post depositional processes. Work by Lachniet *et al*. (2001), comparing microstructures developed within debris flow deposits and subglacial sediments, demonstrated that they share many features in common, including pressure shadows, folds, laminations, shears, faults, water escape structures and ‘galaxy’ or ‘turbate’ structures. Lachniet *et al*. (2001) stress that while deformation microstructures in subglacial sediments can be described in tectonic terms, some of the same structures in debris flow deposits are primary in origin and result from sedimentary processes active during flow and deposition, unaffected by over-riding ice.

This paper describes the micromorphology of a very coarse debris flow deposit occurring within glaciofluvial outwash sediments exposed in the Carstairs area of

Central Scotland (Fig. 1). A comparison is made between this Late Pleistocene debris flow and those that have been described at the terminus of a modern glacier by Lawson (1982) and Lachniet *et al*. (2001) so as to relate the various microstructures present to sedimentary processes active during emplacement. The presence of galaxy or turbate structures within the Westend Wood mass flow deposit, originally considered to be indicative of subglacial deformation (van der Meer 1993), has led to the development of an alternative, or additional model for the development of these structures.

2. Geological setting and field relationships

The Quaternary geology of the Carstairs area in the Midland Valley of Scotland (Fig. 1) is dominated by a sequence of glacial outwash sands and gravels which were deposited in an extensive lake which developed between the uncoupling margins of ice sheets, sourced in the Scottish Highlands, to the north and Southern Uplands, to the south (Thomas & Montague 1977). The glacial outwash sandur was fed from the west by a system of large channels, represented by the Carstairs eskers, with palaeocurrent indicators showing that the main direction of flow was towards the east or southeast. The glacial history of the area has been investigated in detail by Sissons (1961), Boulton (1972), Thomas & Montague (1997) and Bennett & Glasser (1995), amongst others, and will not be described further here.

Westend Wood Quarry (NS 965 468) (Fig. 1), the focus of this study, occurs within the distal parts the glaciofluvial sequence and is located within an area of subdued and irregularly distributed ridges, mounds, channels and basins (landform assemblage B of Thomas & Montague 1997). Boreholes and sections within the quarry show that the sedimentary succession comprises a thick diamicton resting directly upon bedrock, overlain by a coarsening-upwards sequence, *c*. 30 m thick, of laminated silt, fine-sand through fine- to medium-sand into sandy gravel and coarse gravel (Laxton & Nickless 1980; Thomas & Montague 1997). The sequence fines towards the east, passing from laminated sands and massive or cross-bedded pebble gravels containing diamictons, into laminated sands and subordinate granule and pebble gravels, and finally into a thick sequence of parallel-laminated sand, rippled fine sand and mud with occasional rhythmites (see fig 8 of Thomas & Montague 1997). Importantly,

there is no evidence (e.g. over consolidation, pervasive deformation) that these glaciofluvial sediments, and the debris flow deposits which they contain, have been overridden by ice at any time. Consequently, any structures developed within the diamictons and underlying sediments record primary sedimentary processes active during deposition, rather than any glacitectonic induced deformation.

At the eastern end of the Westend Wood Quarry the distal glaciofluvial sands contain a distinctive 2 to 3 m thick bed of diamicton (Fig. 2) which has been interpreted as a debris flow deposit (Thomas & Montague 1997). The very coarse-grained diamicton formed part of an originally laterally extensive deposit (Thomas & Montague 1997) which has now largely been removed by quarrying. The sand dominated sequence below the diamicton is not over consolidated and shows very little evidence of disturbance. The highly heterogeneous diamicton comprises large (≤ 2.0 m in diameter) angular boulders of locally derived basalt (Figs. 2a and b), as well as pebbles and cobbles of altered dacite/rhyolite and microgranite. The clasts are vertically graded and are supported within a variably deformed sandy clay matrix. The matrix varies from massive to stratified near its base; the latter defined by lenticular, streaky-looking bands of silt and clay. Importantly, even the largest boulders present within the diamicton do not penetrate the underlying sediments, suggesting that they were supported within the flow during transport, indicative of a Type 1 debris flow of Lawson (1982). The upper contact of the diamicton is partially obscured, but where exposed appears to have been reworked either during, or prior to the deposition of the overlying sands and gravels. Thomas & Montague (1997), however, reported that elsewhere within the quarry the upper contact of the diamicton was gradational into the overlying rippled sands. The base of the diamicton is sharp and is immediately underlain by a layer of laminated silt, fine-sand and stiff clay 10 to 25 cm thick (Fig. 2a and c). This laminated unit is cross-cut and locally truncated by a 10 to 20 cm thick layer of red sand (Fig. 2b and c) which contains thin stringers of highly deformed clay and diamicton. The massive to locally laminated sands which form the remainder of the sequence below the diamicton are, in general, undeformed. However, a thin (10-15 cm thick) silty horizon (Fig. 2c), which occurs approximately 30 cm below the base of the diamicton, is deformed by a number of small-scale asymmetrical moderately inclined folds which are locally disharmonic to convolute.

3. Micromorphology

Five oriented samples (sample numbers N2593, N2594, N2595, N2596, N2597) were collected from lower part of the diamicton and underlying sands (Fig. 2c) to allow detailed analysis of the microstructures developed during the emplacement of this debris flow and to assess its effect on the underlying sediments. No samples were obtained from within the middle and upper parts of the flow due to the very coarse grained nature of the diamicton. Sample preparation (total time *c*. 10 months) involved the initial replacement of the pore water by acetone which was then progressively replaced by a resin and allowed to cure. Each thin section was cut orthogonal to bedding and to any deformation structures present. The terminology used to describe the various microtextures developed within these sediments in general follows that proposed by van der Meer (1987, 1993) and Menzies (2000).

3.1. Micromorphology of the sediments underlying the diamicton

The fine-grained sands which dominate the sequence below the diamicton are poorly to moderately sorted and possess an open- to moderate-packed clast-supported texture. These sands contain very little clay, reflected in a relatively high intergranular primary porosity. Sand grains are angular to subangular in shape with a low to moderate sphericity and mainly composed of monocrystalline quartz with minor amounts of altered plagioclase and sandstone, basalt and rhyolite rock fragments. Sample N2597 was collected from a deformed silty layer within this sandy sequence (see Fig. 2c). It is composed of finely laminated clayey silt, very fine sand and silty sand. The thin section shows that the deformation occurs within a discrete zone, the upper boundary of which is formed by a prominent bedding surface. It is overlain by undeformed planar to cross-laminated silts and sands (Fig. 3). In the deformed zone the clayey laminae posses a weakly developed bedding-parallel plasmic fabric. This fabric and sedimentary lamination are deformed by a number of moderately to steeply inclined asymmetrical folds (labelled A to C on Fig. 3) and faults. The latter includes a set of steeply dipping normal and reverse faults, as well as gently to moderately dipping thrusts which indicate displacement towards the southeast (Fig. 3). In detail, the faults are relatively diffuse structures, lacking any obvious discrete planes of

dislocation or shear. The folds are separated by curved, moderately dipping thrusts which become progressively steeper to form steeply inclined reverse faults (Fig. 3). Faulting is common within the cores of folds A and B, with the thrusts clearly off-setting bedding on the steep to overturned limbs (Fig. 3). These microstructural relationships suggest that faulting occurred at a later stage in the deformation history than folding. The style of folding varies across the thin section, with folds B and C being more steeply inclined, possessing curved axial surfaces and a more convolute geometry than fold A. Deformation associated with fold C is complex and includes flame-like injection structures and disharmonic parasitic folds (Fig. 3). Silt laminae deformed by this fold have undergone localised liquefaction and homogenisation. A prominent low-angle thrust fault separates the folded unit from an underlying unit of highly deformed laminated silt, clay and fine sand (Fig. 3). These finely laminated sediments are deformed by a relatively tight, rootless recumbent fold which is characterised by small-scale disharmonic parasitic folding around its hinge. The fold is cut by a number of later subvertical, silt-filled hydrofractures.

The laminated clay and silt layer which occurs immediately below the diamicton (see Fig. 2c) is present in samples N2593 (Fig. 4) and N2595 (Fig. 5). In thin section, it is seen to be composed of variably deformed clay, silt and fine-sand (Fig 4). The silt and sand laminae are locally normally graded suggesting that these sediments are the right way up. One of the sandy laminae contains relatively large (≤ 2 mm) coal fragments (Fig. 6a) which are enclosed within a crudely developed skelsepic fabric, defined by the circular arrangement of clay plasma and/or a preferred alignment of detrital muscovite flakes. Deformation within the silt and silty clay laminae includes small-scale folding and thrusting (Fig. 6b), as well as normal and reverse faulting (bottom right of Fig. 5). These folds and faults deform both the sedimentary lamination and a planar, bedding-parallel plasmic fabric that is locally present within clay laminae. The sense of displacement recorded by the thrusts and folds is consistent with an over all sense of shear towards the east or southeast. In sample N2593, the finely laminated sediments are cut by a number of subvertical and subhorizontal hydrofractures (Fig. 4) which were filled by fluidised sand and silty sand (Fig. 6c). The subhorizontal structures typically occur immediately below or within the clay-rich laminae (Fig. 6c), suggesting that the clays temporarily impeded the upward migration of fluidised

sand/pore water. The network of sand-filled fractures are connected to, and were probably fed by material remobilised from the slightly thicker (1-2 cm thick) layer of clean sand visible at the base of the thin section (lower part of Fig. 4).

The laminated clay and silt layer is cross-cut by, and locally truncated against, a distinctive 10 to 20 cm thick unit of laminated, red–brown sand (Fig. 2, 4 and 5). In thin section (samples N2593, N2594, N2595, N2596) this sandy unit is composed of fine- to medium-grained, massive to locally reverse-graded sand, which possesses an open to very open packed texture (Fig. 6d). The locally diffuse, fine-scale bedding or lamination is defined by grain size variation and the relative proportions of a orange-brown to red-brown intergranular clay matrix or 'cement' (see Fig. 5 and lower part of Fig. 7). This 'cement' is a characteristic feature of the sand, with clay-rich laminae possessing a highly dilated, 'cement'- or matrix-supported texture (Fig. 6d) with very little primary porosity. It is composed of a highly birefringent clay which is petrographically similar to clay cutan. The well-developed plasmic fabric present within the clay is distorted around the sand grains which appear to 'suspended' within this 'cement'. In contrast to the clay-rich sand laminae, the interbedded clean sands possess a moderate to high primary intergranular porosity with pore spaces being either completely open or lined by a very thin, birefringent clay rim cement.

The base of the sandy unit is sharp and clearly cuts across both the bedding (Fig. 4) and the deformation structures (lower right hand part of Fig. 5) present within the laminated silt and clay immediately below the diamicton. The upper boundary of the sand is also sharp and truncates the streaky stratification present within the basal part of the diamicton (upper part of Fig. 5, centre of Fig. 7). These microtextural relationships indicate that the formation of the sand layer post-dated deformation within laminated silt and clay unit and deposition of (at least) the basal part of the overlying diamicton. Distorted fragments or augen (up to 12-15 mm in size) of diamicton occur within the sand (sample N2596) and are enclosed within tails of variably deformed and disrupted laminated silt and clay.

3.2. Micromorphology of the diamicton

The basal part of the debris flow deposit was encountered in samples N2594 and N2595 (Figs. 5 and 7 respectively) where it is composed of a stratified, poorly sorted diamicton which possesses a very open packed, matrix-supported texture. The matrix is composed of a red-brown sandy clay (Figs. 7, 8a and b) which locally possesses a weakly developed lattisepic plasmic fabric. Clastic grains included within the diamicton are enclosed within a rim or coating of more clay-rich diamicton which, in some cases, possesses a weakly developed skelsepic plasmic fabric. Circular and arcuate grain alignments (turbate structures), with or without a core stone (Fig. 8a) are variably developed within the matrix. A streaky stratification present within the diamicton is defined by irregular bands or lenses of very finely laminated to highly disrupted silt and clay (Fig. 7). These variably deformed silts and clays are lithologically similar to the laminated silt and clay present immediately below the diamicton. Deformation structures present within these clay-silt lenses include tight to isoclinal, disharmonic folds (including rootless folds), small-scale shears, faults and fractures. A variably developed plasmic fabric is present within the clays. In some bands the clay laminae have undergone microboudinage and occur as angular to locally rounded microboudins within a homogeneous silty matrix (Figs. 8c, d and e). Thin veinlets of silt were also noted along fractures within the clay laminae. The internally disrupted clay and silt lenses may also contain tear drop-shaped (Fig. 8e), rounded (Figs. 8f and 9a) to irregular ‘till pebbles’ (Type 1 and possibly Type 3 till pebbles of van der Meer 1993), as well as wispy looking ribbons or stringers of diamicton (Fig. 8d). Till pebbles were typically observed within the more highly disrupted clay and silt bands, where they occur within a relatively homogeneous silty clay matrix (Fig. 9a). Sand to granule-sized clasts either occur partially ‘embedded’ within the margins of the clay and silt bands (Fig. 8b) or totally ‘included’ within these fine-grained sediments, where they are enclosed within a rim or coating of diamicton (Fig. 9b). The lamination within the clay and silt was observed wrapping around the ‘included’ grains (see Fig. 8b). In the most internally disrupted bands, the original lamination has been overprinted and replaced by variably rounded fragments of clay, sand grains and till pebbles, within a homogeneous clayey silt or silty clay matrix (Figs. 8f, 9a and b).

The boundaries between the laminated bands of clay and silt and the adjacent diamicton are sharp, but irregular in form, being deformed by elongate flame and

cuspate structures (Figs. 9c and 9d, also see Fig. 7). The diamicton contained within the cuspate structures locally possess circular or galaxy textures (Fig. 9d). In some cases, the cuspate structures are relatively deep with a narrow 'neck', and filled by a lobe of diamicton. This 'necking' results in the lobe of diamicton becoming partially included within the clay and silt.

The diamicton adjacent to the clay-silt bands contains irregular to elongate ribbons of silty clay which are aligned parallel to the streaky stratification at the base of the debris flow deposit. This stratification is cut by a number of thin, sand-filled and highly birefringent clay cutan-filled veinlets. The sand-filled veinlets represent hydrofractures and are connected to the underlying red sand unit (see Fig. 7), which also cross-cuts the stratification present in the basal part of the diamicton. These relationships indicate that the sandy unit and sand-filled veinlets post-date the deposition of the diamicton.

5. Interpretation of the microstructures: evidence of basal shearing and liquefaction

It is clear from the above descriptions that the very coarse diamicton which is exposed within Westend Wood Quarry, and which has been interpreted as a debris flow deposit (*cf*. Thomas & Montague 1977), contains microstructures that have also been observed within subglacial diamictons: folds, faults, plasmic fabrics, 'turbate' and 'galaxy' structures (van der Meer 1987, 1983; Menzies 1998, 2000). However, in this case, it is argued that such structures can be interpreted in terms of deformation processes active during emplacement of this debris flow deposit, rather than any subsequent imposed glacitectonic deformation.

5.1. Evidence within the diamicton

Thin sections (N2594, N2595) from the stratified base of the diamicton reveal that it is variably deformed, with the most obvious effects of deformation being concentrated within the lenticular bands of finely laminated silt and clay. This deformation, which produced both ductile and brittle structures, resulted in disharmonic folding, faulting and microboudinage, as well as localised shearing and fabric development within the

clay laminae. In contrast to the clay laminae, the silt appear to be relatively undeformed and homogeneous, with the silt also in filling fractures cutting the adjacent clay laminae. This is consistent with the silty bands having undergone liquefaction during soft-sediment deformation. Apart from a weakly developed lattisepic plasmic fabric and variably preserved arcuate or circular grain arrangements ('turbate' textures), evidence for deformation in the diamicton is limited. This may have resulted from the partitioning of deformation into the relatively weaker clay-silt bands, possibly enhanced by liquefaction of the silts which appears to have accompanied shearing. Consequently, the 'streaky-looking' stratification and associated soft-sediment deformation is interpreted as recording the presence of a basal shear zone to the debris flow. In the shear zone, deformation was focused into the weaker clay and silt layers, with the accompanying liquefaction possibly acting as 'lubricant'. The range of microstructures developed within the basal shear zone are illustrated in Fig. 10.

The clay and silt bands within the stratified base of the diamicton are lithologically the same as the fine-grained sediments which underlie this debris flow deposit. The cusp and flame structures (Figs. 9c and d) developed along the margins of these bands are also considered to have formed in response to basal shearing. These open to locally tight structures disrupt the boundary between the silt-clay bands and adjacent diamicton (Fig. 10). In the least deformed material, this lithological boundary is folded by open, warp-like cusps separated by narrower ridges or incipient flames (Fig. 9c). As deformation continued these features would have progressively tightened, to form deep lobes of diamicton enclosed by highly elongate flames (Fig. 9d). The thin ribbons of silt and clay within the diamicton may represent attenuated flames which have been detached from the silt and clay bands (see Fig. 10). A similar mechanism can be used to explain the presence of till pebbles within the most highly disrupted clay and silt bands. During deformation the narrow 'necks' of deeper cusp structures may be breached, resulting in the detachment of a small lobe of diamicton and the formation of the observed teardrop-shaped (Fig. 8e) and rounded (Figs. 8f and 9a) till pebbles that occur within homogeneous silty clay.

The clay-silt bands also contain sand- and granule-sized clasts coated in a thin rim of diamicton (Fig. 9b). It is possible that these represent dropstones within the original

fine-grained lake sediments or material shed from the front of the advancing debris flow. Alternatively, these coated grains may have been incorporated into the finer grained sediments during deformation. Sand grains and granules ‘embedded’ along the margins of the clay and silt bands and distorting the lamination within these fine-grained sediments have been noted (Fig 8b). During deformation these grains may become progressively incorporated into, and eventually completely enclosed within the clay and silt bands. The result would be the transfer of material from the diamicton into the clay and silt. During this process minor amounts of the matrix to the diamicton may adhere to the clast resulting in the formation of coated grains. The combined effects of detachment of deformed flames and cusps, and liquefaction and mobilisation of the silts during deformation, would have led to breakdown of the clay and silt bands and mixing/incorporation of these fine-grained sediments into the body of the diamicton.

5.2. Evidence below the diamicton

Field and micromorphological analysis show that the predominantly sandy sediments which underlie the diamicton show very little evidence of disturbance. Evidence of deformation, where present, is confined to the folding and faulting of a 10 to 25 cm thick bed of laminated silts and clays immediately below the diamicton (N2593, N2595), and a zone of soft-sediment deformation within a silty layer (N2597) approximately 30 cm below the base of this deposit (see Fig. 2c). This suggests that the deformation was preferentially partitioned into these finer grained sediments. The asymmetry of the folds and displacement on the thrusts within these zones of increased deformation all record a sense of shear towards the south-east, suggesting that both of these structures were formed during the same deformation event. Microstructural relationships indicate, however, that faulting post-dated folding (see Fig. 3), with the thrusts and related reverse faults possibly accommodating further shortening as deformation continued. This deformation event probably resulted from overriding by the debris flow during emplacement, with the kinematics obtained from the microstructures suggesting a direction of transport towards the southeast.

The locally disharmonic nature of the folds and associated liquefaction and water escape (e.g. flame–like injection features, sand and silt filled hydrofractures) indicates

that these sediments possessed a relatively high water content during, at least, the early stages of deformation. However, the water content must have decreased as deformation continued, to allow brittle faulting to occur. This suggests that pore water content and/or pressure fluctuated during the emplacement of the debris flow deposit. The network of vertical and subhorizontal silt- and sand-filled veins (hydrofractures) (see Figs. 4, 6c and 10) developed during the dewatering of these sediments. The required increase in pore water pressure which lead to hydrofracturing may record an increase in the overburden pressure caused by the emplacement of the debris flow. The subhorizontal, bedding-parallel veins, which occur within or immediately below clay-rich laminae, probably resulted from these fine-grained sediments temporarily impeding hydrofracture development and the upward migration of fluidised sand/pore water. This fluidised material would then be forced to spread laterally until the cohesive strength of the clay was exceeded and upward migration of the fluidised sand could be reinstated. Microtextural evidence preserved in sample N2597, indicates that dewatering post-dated folding, but pre-dated faulting as there is no evidence of the sand-filled hydrofractures having been injected along the thrusts.

In both the field and thin section, the boundary between the diamicton and the underlying sedimentary sequence is cross-cut by a layer of laminated red sand (Fig. 2c). The upper and lower contacts of this sandy unit clearly cross-cut the ‘streaky-looking’ stratification within the basal part of the diamicton (Figs. 5 and 6), as well as the lamination and deformation structures developed within the underlying silts and clays (Figs. 4 and 5). Furthermore, veins (hydrofractures) filled by this sand were also observed intruding the base of the diamicton (see Fig. 7) indicating that pore water pressure locally exceeded the cohesive strength of this deposit. These relationships indicate that the introduction of this sand layer post-dated the deposition of at least the basal part of the diamicton and deformation associated with the incoming of this debris flow deposit. The open to very open packed sand possesses a distinctive with a locally developed ‘cement’- or matrix-supported texture (Fig. 6d). The highly birefringent clay ‘cement’ is petrographically similar to a clay cutan, with the overall texture of the sand suggests that it was introduced whilst the sediment was in a highly dilated (water saturated) state. Consequently, rather than being a part of the primary sedimentary sequence, this sand layer is interpreted as having been injected along the boundary between the diamicton and underlying sediments. The laminated nature of

the sand suggests that injection was not a single event, but occurred as a series of pulses.

6. Model for the emplacement of the diamicton

The diamicton exposed in Westend Wood Quarry may be broadly classified as a Type 1 flow of Lawson (1982), in which the large boulders of basalt were supported within a relatively cohesive matrix during transport. An idealised section through the debris flow is illustrated in Fig. 11. In Type 1 debris flows, movement is concentrated within a relatively thin (few centimetres thick) basal shear zone with little, if any, internal deformation within the overriding debris flow contributing to forward motion (Lawson 1982; Lachniet *et al*. 2001). The evidence of soft-sediment deformation and stratified nature of the lower part of the diamicton from Westend Wood Quarry are consistent with the development of a basal shear zone (Fig. 11). Deformation within this zone was focused into the weaker clay and silt bands which define the 'streaky-looking' stratification. At the base of the diamicton, liquefaction of the silty laminae during deformation would have resulted in the lowering of the cohesive strength of the sediments within the shear zone, acting as a 'lubricant', and aiding transport of the overriding debris flow.

The laminated silts and clays may have originally been lacustrine deposits incorporated into the base of the overriding debris flow. Alternatively, these clays and silts may have been deposited as a very fine slurry immediately in front of the advancing debris flow (Fig. 11) by meltwater or by expelled pore water flowing over the top of the flow. Shearing at the base of the debris flow, coupled with the liquefaction of the silty laminae may have aided in the 'mixing' of these sediments into the matrix of the diamicton.

As previously stated, both field and micromorphological studies show that the predominantly sandy sediments which underlie the diamicton show very little evidence of disturbance. Deformation, where, present, was partitioned into the weaker, finer grained sediments resulting in soft-sediment deformation and localised liquefaction. The fluidised sands and silts formed a network of hydrofractures which

cross-cut earlier ductile structures. This network of veins may have fed the red sand injected along the boundary between the diamicton and underlying glaciofluvial sands (Fig. 11). This sand layer cross-cuts and truncates the deformation structures developed within the clay-rich sediments immediately below the diamicton, and the stratification at the base of this deposit. The clayey nature of the diamicton would have retarded the upward migration of the fluidised sand, forcing it to spread laterally along the base of the debris flow deposit (Fig. 11). It is possible that this fluidised sand layer may have resulted in the decoupling of the debris flow from its bed, leading to a reduction of the amount of shear transmitted into the sediments underlying the diamicton. If correct, this would marked a change in the mode of emplacement of the mass flow; from an initial transport mechanism dominated by basal shearing, to model in which the diamicton is decoupled from its bed with displacement being taken up along the fluidised sand layer (see Fig. 11).

Lawson (1982) found that debris flows developed at the terminus of the Matanuska Glacier led to the deformation (folding, thrusting) of the unconsolidated sediments revealed during ice wastage. These sediments are locally oversaturated and exhibit evidence of rapid water expulsion through vertical and lateral channels or fractures. In some of these modern debris flows, Lawson (1982) demonstrated that the basal shear zone was oversaturated and often composed of greater than 50% water by volume; the overriding plug, however, was just saturated or undersaturated. The interpretation of a water saturated basal zone and decoupling of the debris flow in Westend Wood Quarry may be supported by the relatively undeformed nature of the underlying glaciofluvial sediments. Thomas & Montague (1997) suggested that the debris flow at Westend Wood Quarry slumped into the margin of the lake, so the underlying glaciofluvial sediments would have already possessed a relatively high porewater content. The increase in pore water content within the basal zone of the mass flow may have occurred due to dewatering of these already wet sediments and, possibly to a lesser extent, the overriding flow.

7. The origin of ‘galaxy’ or ‘turbate’ structures

‘Galaxy’ and ‘turbate’ structures have been described from both subglacial diamictons (van der Meer 1993, 1997; Menzies 1998, 2000; Khatwa & Tulaczyk 2001) and

debris flow deposits (Lachniet *et al*. 1999; Lachniet *et al*. 2001; this study). Although originally considered to be indicative of subglacial deformation (van der Meer 1993), it is more than likely that these rotational deformation structures (van der Meer 1993; Menzies *et al*. 1997) share a common mode of origin and are therefore not diagnostic of subglacial processes. They comprise a circular, tangential arrangement of grains with, or without, a central core stone formed by a larger clast (Fig. 12). In some cases there may be a concentration of fines (e.g. clay) within the matrix immediately adjacent to the core stone (Fig. 12). If clay-rich, this 'coating' may possess a variably developed skelsepic plasmic fabric. The lack of asymmetry and circular nature of 'galaxy' structures suggests that they were free to rotate through at least 360°. In the model for the formation of these features proposed by van der Meer (1997), the subglacially deforming diamicton is thought to be made up of rotational elements or wheels, consisting of a nucleus alone, or with spiralling arms (galaxy structures) of finer grains. Van der Meer (1987) suggested that these rotational elements would also enable clast mobility within the deforming diamicton, with finer grains moving from one wheel to the next (see figs. 2 and 3 of van der Meer 1997).

In many diamictons, 'galaxy' structures are either absent or only poorly developed. This suggests that the process by which these structures form is either very localised or transitory in nature, allowing the overprinting of earlier developed features as deformation continued. One such transient form of rotational deformation may be caused by turbulent rather than laminar flow within the diamicton. Turbulence may occur immediately adjacent to large, slowly moving or immobile pebbles or boulders, where flow within the matrix is deflected around these clasts (Fig. 13a). Lawson (1982) noted that brief, transient periods of turbid mixing occurred within debris flows as they passed over irregularities within the bed, or a change in angle of its slope (Fig. 13b). Turbulent flow would lead to the development of transitory 'rotational cells' which may nucleate upon, and lead to the rotation of, finer grained clasts present within the matrix of the diamicton (Fig. 14). The rotating clast will effectively entrain the adjacent matrix and become enclosed within a spherical to ellipsoidal envelope of actively rotating finer grained material. These 'rotational cells' will expand, propagating both laterally and vertically as they migrate through the diamicton (Fig 14, Stage 1) away from the mechanical instability which first initiated this form of rotational deformation. Variations in the rheological properties of the

matrix (such as water content) could lead to distortion (Fig. 14, Stage 2), fragmentation and even collapse of the 'rotational cell' (Fig. 14, Stage 3). Once the driving force maintaining the 'rotating cell' begins to dissipate, the integrity of the circular or galaxy structure will be lost. The earlier-formed galaxy, circular or turbate structures will then fragment and be progressively overprinted as deformation associated with laminar flow is reinitiated.

8. Conclusions

Micromorphological analysis of a very coarse debris flow deposit exposed within Westend Wood Quarry, Carstairs (Central Scotland) has revealed microstructures (folds, faults, plasmic fabrics) which have also been recorded within subglacial diamictons. However, by comparing this diamicton to previously published data on debris flows formed at the terminus of modern glacier it is possible to relate these microstructures to deformation processes active during emplacement of the debris flow. These processes include: the formation of a basal shear zone; the deformation and mixing of fine-grained sediments incorporated into the base of the overriding debris flow; and the recognition of features associated with liquefaction, sediment remobilisation and water escape, which developed in response to increasing overburden pressure during the emplacement of the debris flow.

The development of a fluidised sand layer near to the interface between the debris flow diamicton and the underlying wet sediments may have resulted in the decoupling of the debris flow from its bed. This was associated with a marked change in the mode of emplacement of the mass flow; from an initial transport mechanism dominated by basal shearing, to fluidisation and continued displacement along a thin layer at its base. The latter would have resulted in a reduction of the amount of shear transmitted into the bed by the active debris flow and explain the relatively undisturbed nature of the underlying sediments.

The presence of 'galaxy' or 'turbate' structures within both debris flows and subglacial diamictons suggests they share a common origin and are therefore not diagnostic of a single depositional environment. These structures are thought to develop in response to transitory rotational deformation, possibly associated with

turbulent flow in the matrix of the sediments. The occurrence of common microstructures within diamictons formed in a range of depositional settings highlights the importance of using micromorphological analysis in conjunction with macroscopic field sedimentological and structural studies to fully elucidate their genesis.

9. Acknowledgements

The work forms part of the Midland Valley Project of the British Geological Survey's Integrated Geological Survey (North) programme. David Oates is acknowledged for his expertise in making thin section of even the most poorly consolidated sediments. Jon Merritt, Clive Auton, Tom Bradwell and Maxine Akhurst are acknowledged for their comments and discussions of an earlier draft of this paper. Simon Carr and Jim Rose are also thanked for their constructive reviews. This paper is published with the permission of the Executive Director of the British Geological Survey (NERC).

10. References

Bennett, M. and Glasser, N. 1995. Process, bar morphology, and sedimentary structures on braided outwash fans, northeast Gulf of Alaska. *In* Jopling, A.V. & McDonald, B.C. (eds) *Glaciofluivial and Glaciolacustrine Sedimentation*. Special Publication of the Society of Economic Palaeontologists and Mineralogists. **23,** 193-222.

Boulton, G.S. 1972. Modern Artic glaciers as a depositional model for former ice-sheets. *Journal of the Geological Society of London*. **128,** 361-393.

Carr, S.J. Haflidason, H. and Sejrup, H.P. 2000. Micromorphological evidence supporting Late Weichselian glaciation of the Northern North Sea. *Boreas*. **29,** 315-328.

Harris, C. 1998. The micromorphology of paraglacial and periglacial slope deposits: a case study from Morfa Bychan, west Wales, UK. *Journal of Quaternary Science*. **13,** 73-84.

Hart, J. and Rose, J. 2001. Approaches to the study of glacier bed deformation. *Quaternary International*. **86,** 45-58.

Khatwa, A. and Tulaczyk, S. 2001. Microstructural interpretations of modern and Pleistocene subglacially deformed sediments: the relative role of parent material and subglacial process. *Journal of Quaternary Science*. **16,** 507-517.

Lachniet, M.S., Larson, G.J., Strasser, J.C., Lawson, D.E. and Evenson, E.B. 1999. Microstructures of glacigenic sediment flow deposits, Matanuska Glacier, Alaska. *In* Mickleson, D.M. & Attig, J.W. (eds). *Glacial Processes Past and Present. Geological Society of America, Special Paper*. **337,** Boulder, CO.

Lachniet, M.S., Larson, G.J., Lawson, D.E. Evenson, E.B. and Alley, R.B. 2001. Microstructures of sediment flow deposits and subglacial sediments: a comparison. *Boreas*. **30,** 254-262.

Laxton, J.L. and Nickless, E.F.P. 1980. *The sand and gravel resources of the country around Lanark, Strathclyde Region. Description of 1:25,000 sheet NS94 and part of NS84*. Mineral Assessment Report of the Institute of Geological Sciences. pp 49.

Lawson, D.E. 1982. Mobilization, movement and deposition of active subaerial sediment flows, Matanuska Glacier, Alaska. *Journal of Geology*. **90,** 279-300.

Menzies, J. 1998. Microstructures within subglacial diamictons. *In* Kostrzewski, A. (ed) *Relief and Deposits of Present-day and Pleistocene Glaciation of the Northern Hemisphere – selected problems*. Adam Michiewicz University Press, Poznan, Geography Series. **58,** 210-216.

Menzies, J. 2000. Micromorphological analyses of microfabrics and microstructures indicative of deformation processes in glacial sediments. *In* Maltman, A. J., Hubbard, B. & Hambrey, J. M. (eds) *Deformation of Glacial Materials*. Geological Society, London, Special Publication. **176,** 245-257.

Menzies, J. and Maltman, A.J. 1992. Microstructures in diamictons – evidence of subglacial bed conditions. *Geomorphology*. **6,** 27-40.

Menzies, J, Zaniewski, K., Dreger, D. 1997. Evidence from microstructures of deformable bed conditions within drumlins, Chimney Bluffs, New York State. *Sedimentary Geology*. **111,** 161-176.

Phillips, E.R. and Auton, C.A. 2000. Micromorphological evidence for polyphase deformation of glaciolacustrine sediments from Strathspey, Scotland. *In* Maltman, A.J., Hubbard, B. and Hambrey, M.J. (eds). *Deformation of Glacial Materials*. Geological Society, London, Special Publications. **176,** 279-292.

Seret, G. 1993. Microstructures in thin sections of several kinds of till. *Quaternary International*. **18,** 97-101.

Sissons, J.B. 1961. The central and eastern parts of the Lammermuir - Stranraer moraine. *Geological Magazine*. **98,** 380-392.

Thomas, G.S.P. and Montague, E. 1997. The morphology, stratigraphy and sedimentology of the Carstairs Esker, Scotland, U.K. *Quaternary Science Reviews.* **16,** 661-674.

van der Meer, J.J.M. 1987. Micromorphology of glacial sediments as a tool in distinguishing genetic varieties of till. *In* Kujansuu, R. and Saarnisto, M (eds). *INQUA Till Symposium, Finland 1985*. Geological Survey of Finland, Special Paper. **3,** 77-89.

van der Meer, J.J.M. 1993. Microscopic evidence of subglacial deformation. *Quaternary Science Reviews*. **12,** 553-587.

van der Meer, J.J.M. 1997. Particle aggregate mobility in till: microscopic evidence of subglacial process. *Quaternary Science Reviews*. **16,** 827-831.

van der Meer, J.J.M. and Laban, C. 1990. Micromorphology of some North Sea till samples, a pilot study. *Journal of Quaternary Science*. **5,** 95-101.

van der Wateren, F.M., Kluiving, S.J. and Bartek, L.R. 2000. Kinematic indicators of subglacial shearing. *In* Maltman, A.J., Hubbard, B. and Hambrey, M.J. (eds). *Deformation of Glacial Materials*. Geological Society, London, Special Publications. **176,** 259-278.

Figures

Fig. 1. Simplified geological map of part of the Carstairs district (central Scotland) showing the location of Westend Wood Quarry. Inset maps show the location of study area within the Midland Valley of Scotland.

Fig. 2. (a) The sand dominated glaciofluvial sequence exposed in Westend Wood Quarry containing a very coarse diamicton which is characterised by the presence of large boulders of alkali basalt. **(b)** Lower boundary of the diamicton which is separated from the underlying sand-dominated sequence by a relatively thin layer of deformed laminated clays and silt, cross-cut by a layer of red sand. **(c)** Simplified lithological log through the sequence showing the relative positions of the 5 samples (N2593, N2594, N2595, N2596, N2597) collected for micromorphological analysis.

Fig. 3. Thin section of sample N2597 which is characterised by soft-sediment deformation (folding, faulting) of laminated fine-sand, silt and clay. Deformation is most intense in the lower and central parts of the section, with these sediments also showing evidence fluidisation and remobilisation of the silt to fine-sand laminae. Folds labelled A, B and C referred to in text. (Scale bar = 10 mm) (see Fig. 2c for the location of this sample)

Fig. 4. Thin section of a sample (N2593) of the laminated silt, fine sand and clay, and cross-cutting laminated sand exposed immediately below the diamicton. These laminated sediments are cut by a number of sand- and/or silt filled veins (hydrofractures) (Scale bar = 10 mm). Also shown are the locations of the photomicrographs show in Figs. 6a, b, c, and d. (see Fig. 2c for the location of this sample)

Fig. 5. Thin section of sample N2595 showing the relationship between the diamicton and laminated sand layer. This sand clearly cross-cuts earlier formed microfaults within the underlying laminated silt and clay present at the base of the section and the 'streaky-looking' stratification developed within the diamicton. Also shown are the locations of the photomicrographs show in Figs. 8e and 9b, c and d. (Scale bar = 10 mm) (see Fig. 2c for the location of this sample)

Fig. 6. Photomicrographs showing: **(a)** Laminated clay and silty sand truncated at the erosive base of a layer of silt containing subangular to subrounded fragments of coal (N2593; PPL; scale bar = 2 mm); **(b)** Small-scale folding and thrusting of a normally graded silt lamina (N2593; PPL; scale bar = 2 mm); **(c)** Network of vertical and subhorizontal (bedding-parallel) sand-filled hydrofractures (N2593; plane polarised light (PPL); scale bar = 2 mm); and **(d)** Poorly sorted sand with an open packed, 'cement'- or matrix-supported texture. The 'cement' or matrix is composed of a distinctive orange-brown clay cutan (N2593; PPL; scale bar = 1 mm).

Fig. 7. This section (N2594) showing the boundary between the stratified base of the diamicton and underlying laminated matrix-poor sand. This sand unit clearly cross-cuts the streaky looking stratification (defined by highly deformed silt and clay bands) present at the base of the diamicton (Scale bar = 10 mm). Also shown are the locations of the photomicrographs show in Figs. 8a, b, c, d and f, and 9a. (see Fig. 2c for the location of this sample)

Fig. 8. Photomicrographs showing: **(a)** An open cusp structure deforming the boundary of a silt and clay band within the stratified diamicton. The rhyolite fragment present within this cuspate fold is enclosed within a weakly developed arcuate to circular arrangement ('galaxy' or 'turbate' structure) of finer grained clasts of monocrystalline quartz and feldspar (N2594; PPL; Scale bar = 1 mm); **(b)** Hematised sandstone clast partially included or embedded within the margin of a disrupted silty layer. The fine-scale lamination within the silt-clay layer is deformed/deflected around this lithic clast (N2594; PPL; Scale bar = 1 mm); **(c)** Highly disrupted silt and clay. Elongate fragments or microboudins of the clay laminae occur within a homogenous apparently undeformed silty matrix (N2594; PPL; Scale bar = 2 mm); **(d)** Highly deformed and disrupted silt and clay layer within the basal, stratified part

of the diamicton. This highly disrupted and partially homogenised layer also contains elongate wispy-looking stringers of diamicton (N2594; PPL; Scale bar = 2 mm); **(e)** Teardrop-shaped till pebble in a silty clay matrix (N2595; PPL; Scale bar = 1 mm); **(f)** Homogeneous silty clay band containing fragments of clay (muds clasts) sand grains, lithic clasts and till pebbles derived from the adjacent diamicton. Also note the presence of circular grain alignments within this silty layer (N2595; PPL; Scale bar = 1 mm).

Fig. 9. Photomicrographs showing: **(a)** Homogeneous silty clay layer containing subangular to subrounded fragments of clay (mud clasts) and till pebbles derived from the adjacent diamicton layer. Also note presence of poorly developed circular and arcuate arrangements of clasts within this homogenised silty clay (N2595; PPL; Scale bar = 2 mm). **(b)** Large fragment of sandstone enclosed within a rim or coating of fine-gained material similar to the matrix of the diamicton (N2595; PPL; Scale bar = 2 mm). **(c)** Cusp and flame structures deforming the boundary between a silt and clay band and the adjacent diamicton. The matrix of the diamicton also contains circular and arcuate grain alignments (‘turbate’ structures) (N2594; PPL; Scale bar = 2 mm). **(d)** Elongate flame and cusp structure deforming boundary of a disrupted silt and clay layer within the stratified diamicton. Also note the presence of circular and arcuate clast arrangements within the diamicton associated with the cuspate structure (N2594; PPL; Scale bar = 1 mm).

Fig. 10. Diagram showing the range of microstructures developed within the stratified base of the diamicton. Also shown is a model for the progressive development of cusp and flame structures, and the inclusion of till pebbles within the highly disrupted and homogenised clay-silt bands. (not to scale)

Fig. 11. Schematic cross section (not to scale) through the debris flow deposit exposed in Westend Wood Quarry showing the presence of a stratified basal shear zone within the diamicton. Micromorphological revealed that the sediments underlying the diamicton are intruded by a network of sand- and silt-filled

hydrofractures. Inset shows the detail of the sediments exposed immediately below the diamicton.

Fig. 12. Diagram showing the idealised morphology of circular, arcuate and 'galaxy'-like grain arrangements associated with rotational deformation within diamictons: **(a)** concentric arrangement of grains around a large clast; **(b)** concentric arrangement of grains without 'core stone'; **(c)** spiral arrangement of grains around larger clast; and **(d)** arcuate clusters or aggregates of grains.

Fig. 13. Model for the development of galaxy or turbate rotational deformation structures associated with localised, transient turbulent flow adjacent to: **(a)** large immobile boulder; and **(b)** an irregularity in underlying the bed.

Fig. 14. Diagram showing the progressive development and collapse of 'rotating cells' associated with grain rotation.

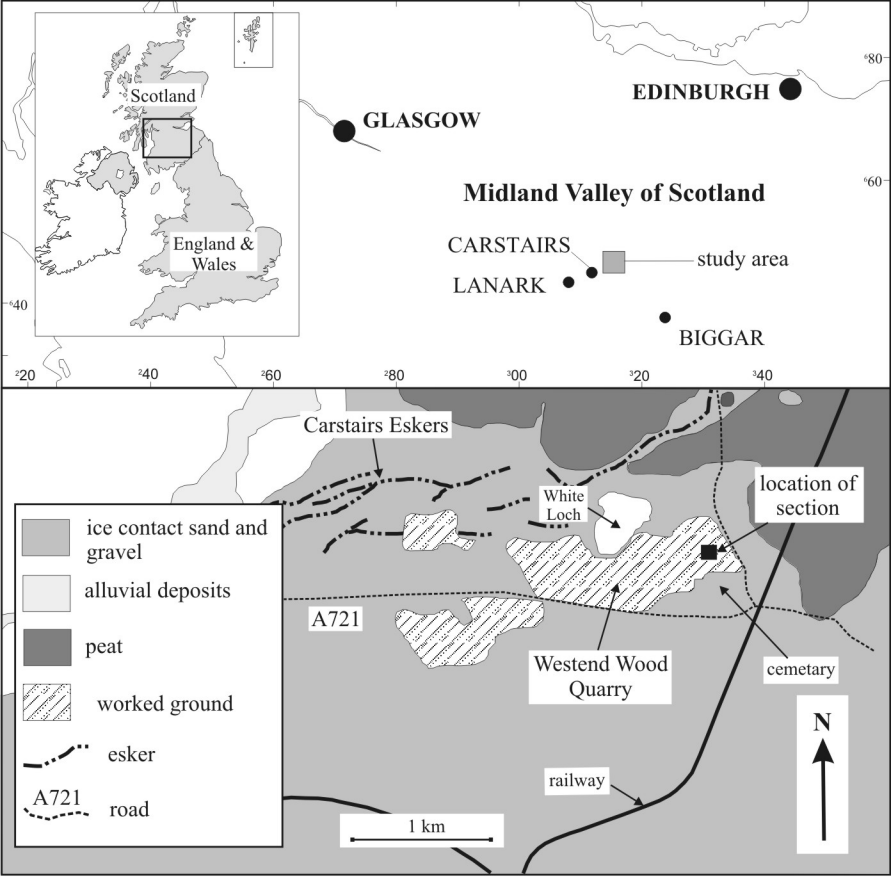
Scotland
England & Wales
GLASGOW
EDINBURGH
Midland Valley of Scotland
CARSTAIRS
LANARK
study area
BIGGAR
Carstairs Eskers
White Loch
location of section
A721
Westend Wood Quarry
cemetary
railway
N
1 km
ice contact sand and gravel
alluvial deposits
peat
worked ground
esker
A721
road

Figure 1.

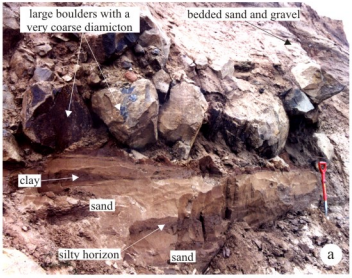
large boulders with a very coarse diamicton
bedded sand and gravel
clay
sand
silty horizon
sand
a

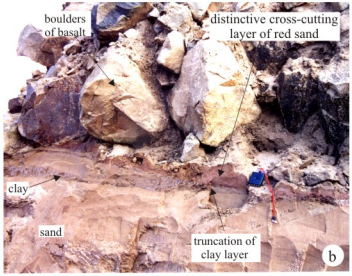
boulders of basalt
distinctive cross-cutting layer of red sand
clay
sand
truncation of clay layer
b

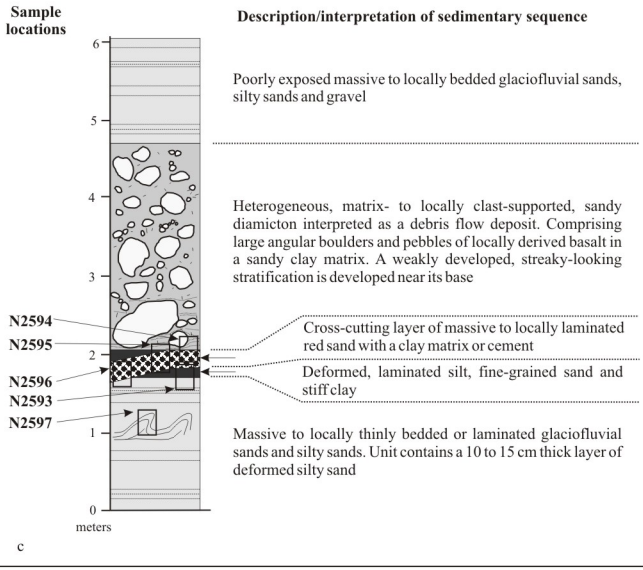
Sample locations
Description/interpretation of sedimentary sequence
6
5
4
3
2
1
0
meters
N2594
N2595
N2596
N2593
N2597
Poorly exposed massive to locally bedded glaciofluvial sands, silty sands and gravel
Heterogeneous, matrix- to locally clast-supported, sandy diamicton interpreted as a debris flow deposit. Comprising large angular boulders and pebbles of locally derived basalt in a sandy clay matrix. A weakly developed, streaky-looking stratification is developed near its base
Cross-cutting layer of massive to locally laminated red sand with a clay matrix or cement
Deformed, laminated silt, fine-grained sand and stiff clay
Massive to locally thinly bedded or laminated glaciofluvial sands and silty sands. Unit contains a 10 to 15 cm thick layer of deformed silty sand
c

Figure 2

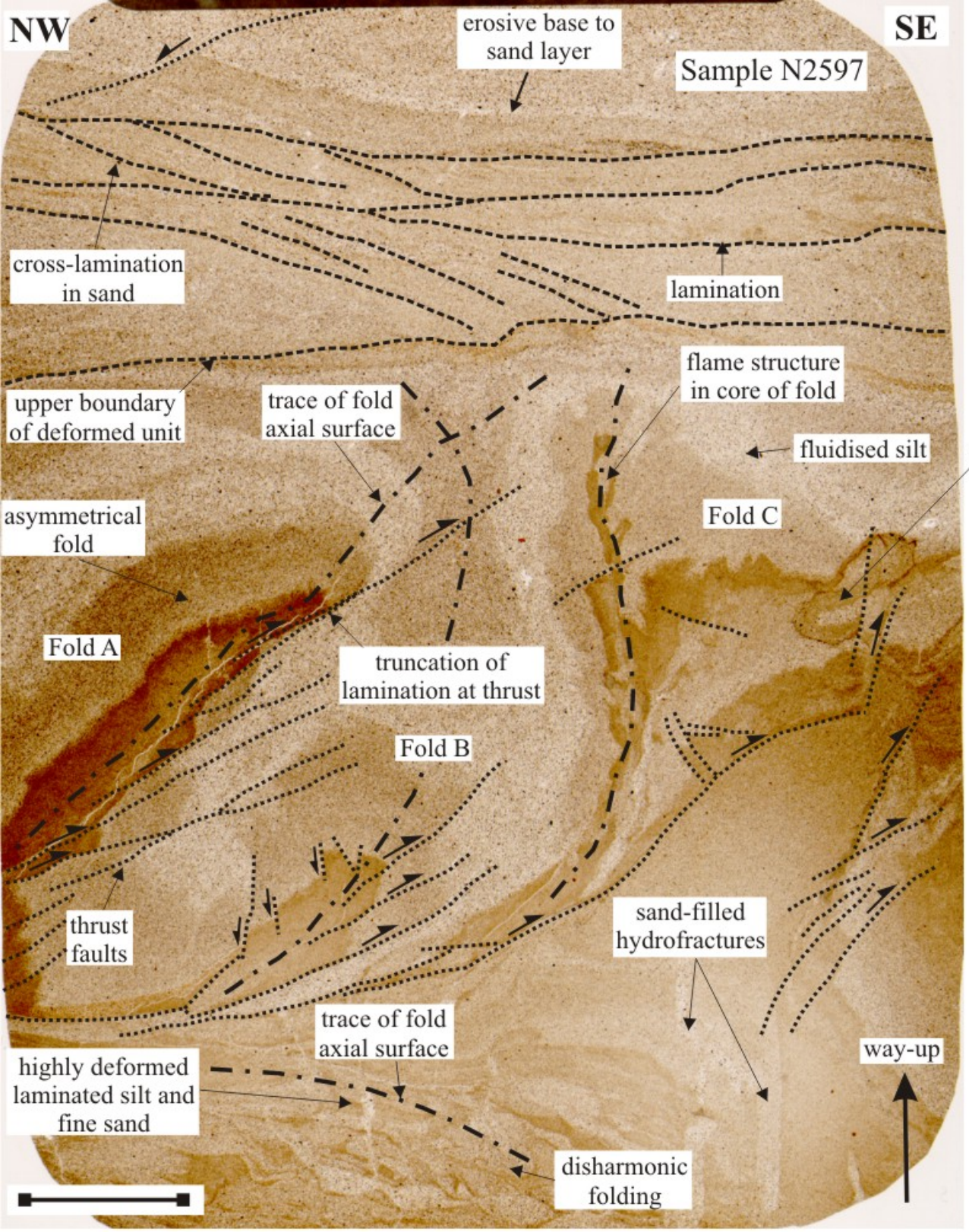
NW
SE
erosive base to sand layer
Sample N2597
cross-lamination in sand
lamination
upper boundary of deformed unit
trace of fold axial surface
flame structure in core of fold
fluidised silt
disharmonic folding
asymmetrical fold
Fold C
Fold A
truncation of lamination at thrust
Fold B
thrust faults
sand-filled hydrofractures
trace of fold axial surface
highly deformed laminated silt and fine sand
way-up
disharmonic folding
homogeneous sand
undeformed, parallel laminated and cross laminated fine sand
folded and faulted laminated clay, silt and fine sand with liquefaction of silt and fine sand associated with soft-sediment deformation
highly deformed, laminated silt, clay and fine sand

Figure 3.

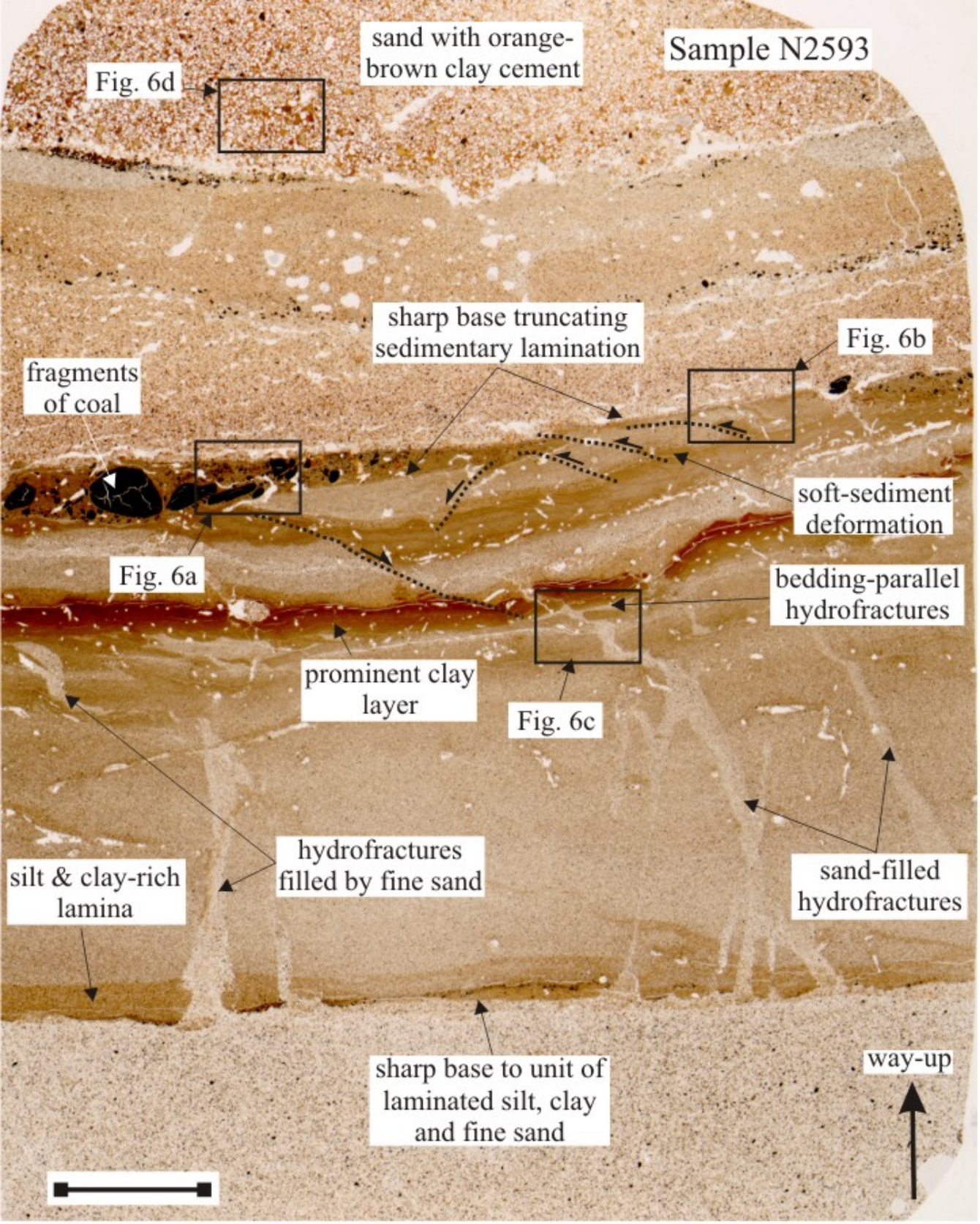

laminated sand with variably developed open-packed cement supported texture

laminated fine sand, silt and clay locally cut by sand- to silt-filled hydrofractures

homogeneous, clean sand

Figure 4.

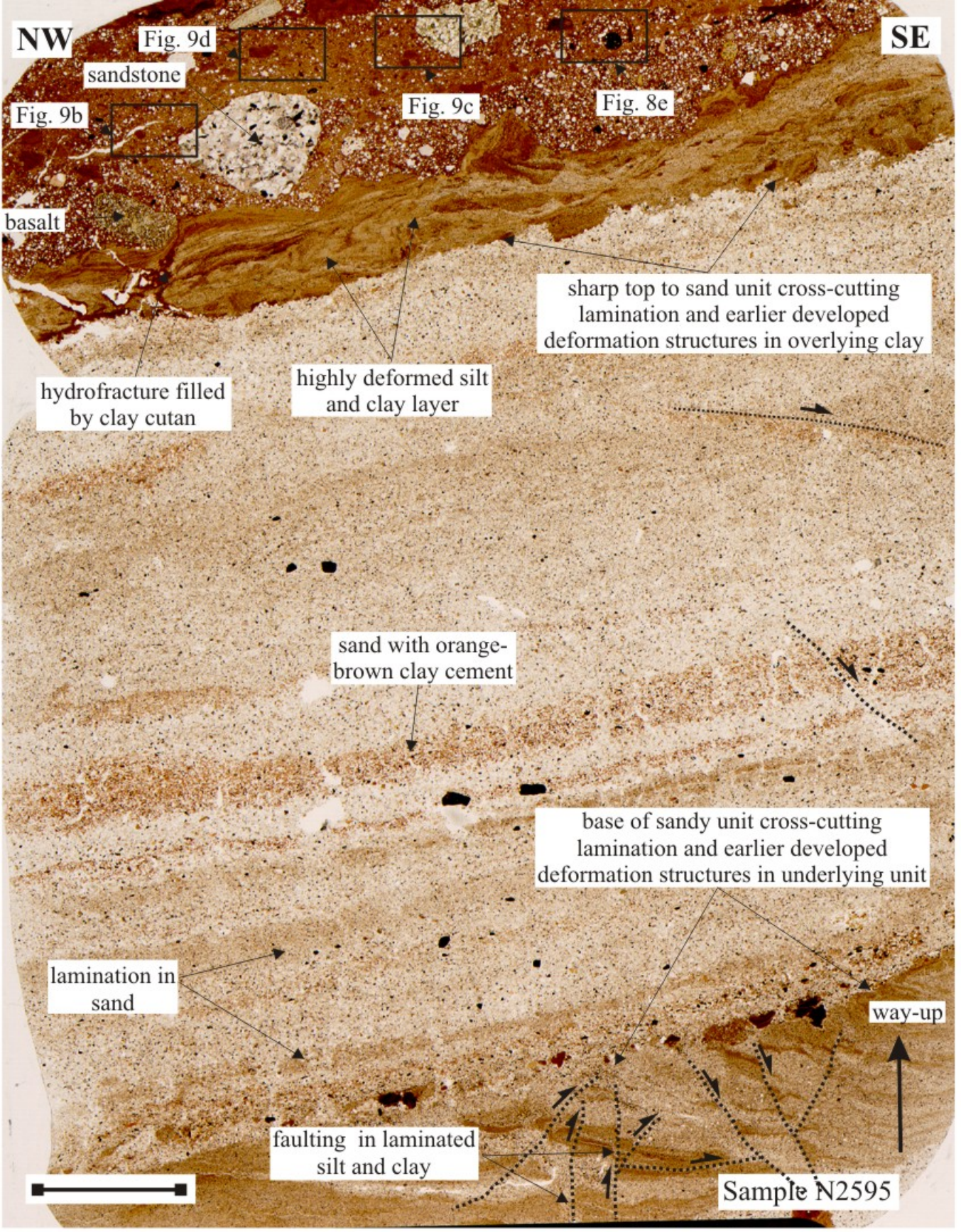
NW
SE
Fig. 9d
sandstone
Fig. 9b
Fig. 9c
Fig. 8e
basalt
stratified base of diamicton
sharp top to sand unit cross-cutting lamination and earlier developed deformation structures in overlying clay
hydrofracture filled by clay cutan
highly deformed silt and clay layer
laminated matrix-poor sand with locally developed clay cement
sand with orange-brown clay cement
base of sandy unit cross-cutting lamination and earlier developed deformation structures in underlying unit
lamination in sand
way-up
deformed laminated silt and clay
faulting in laminated silt and clay
Sample N2595

Figure 5.

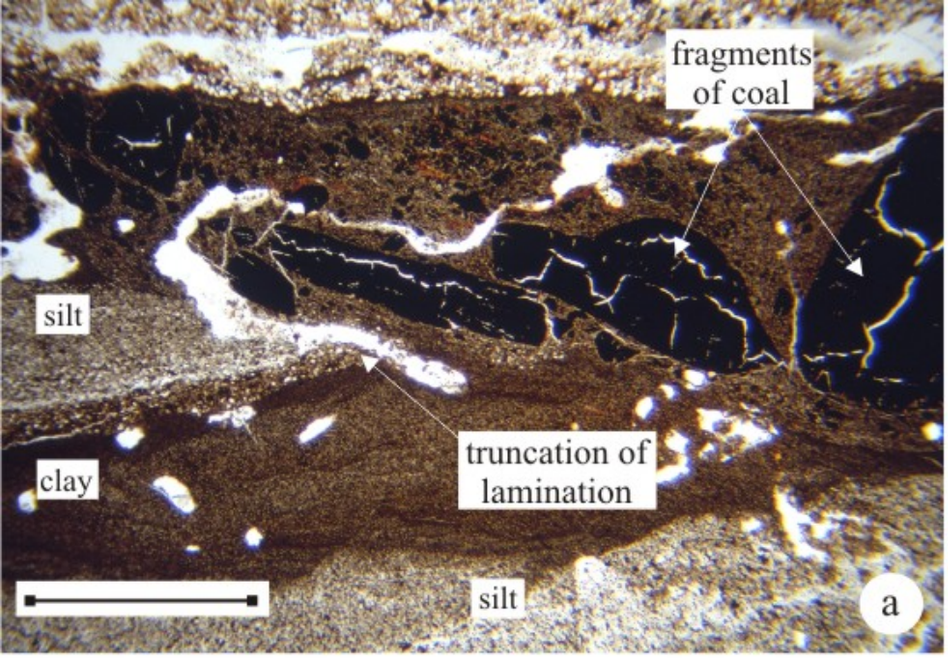

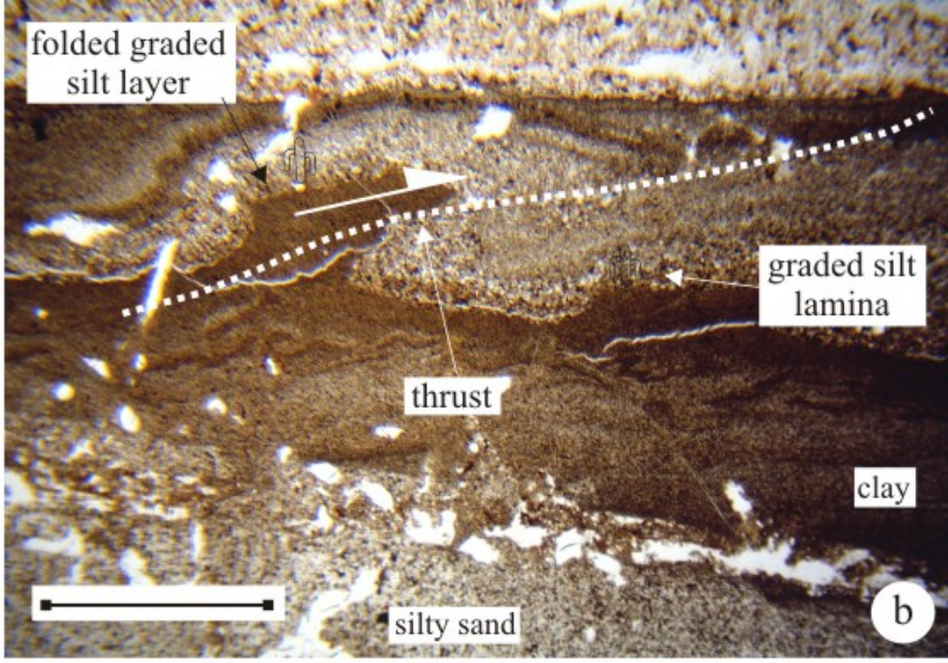

way-up

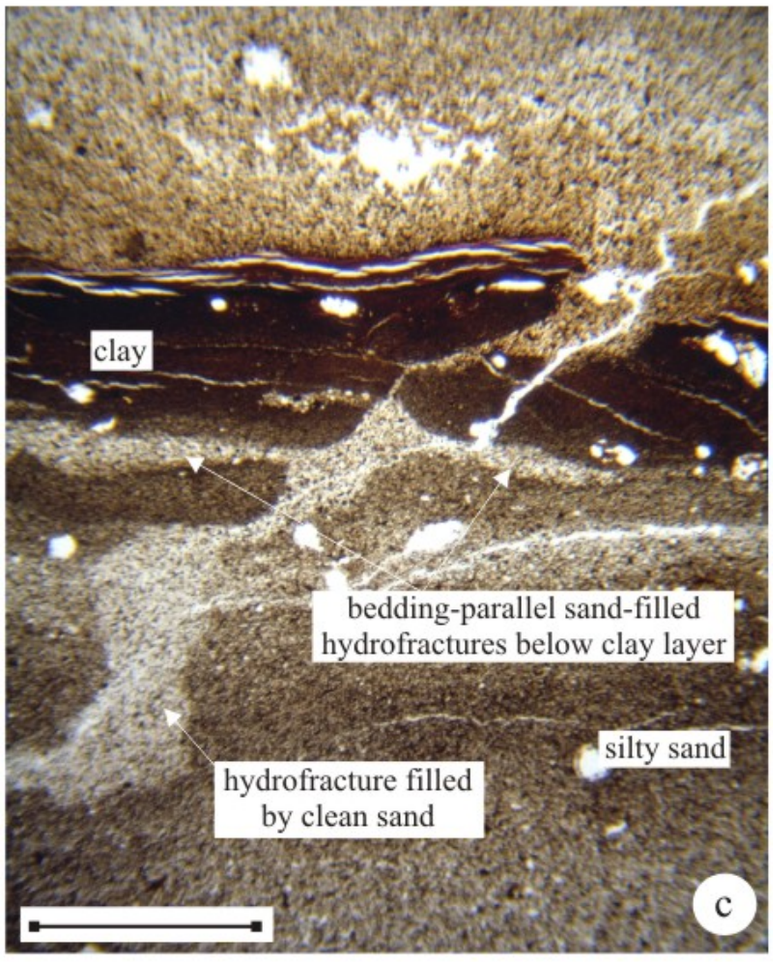

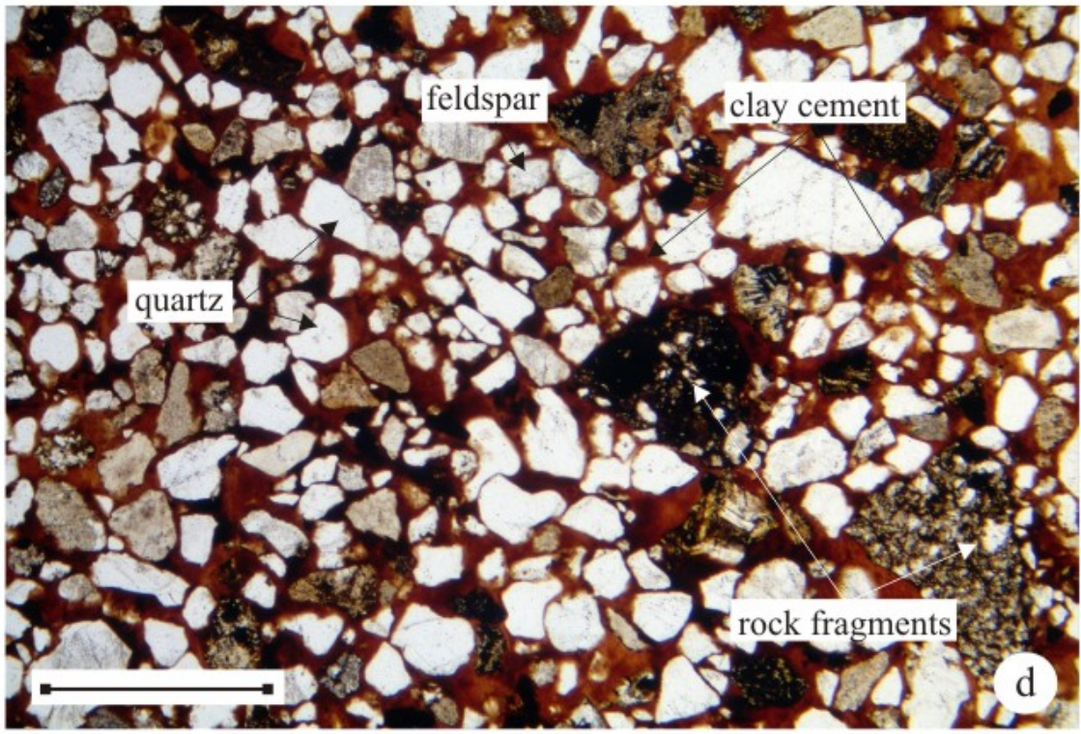

Figure 6.

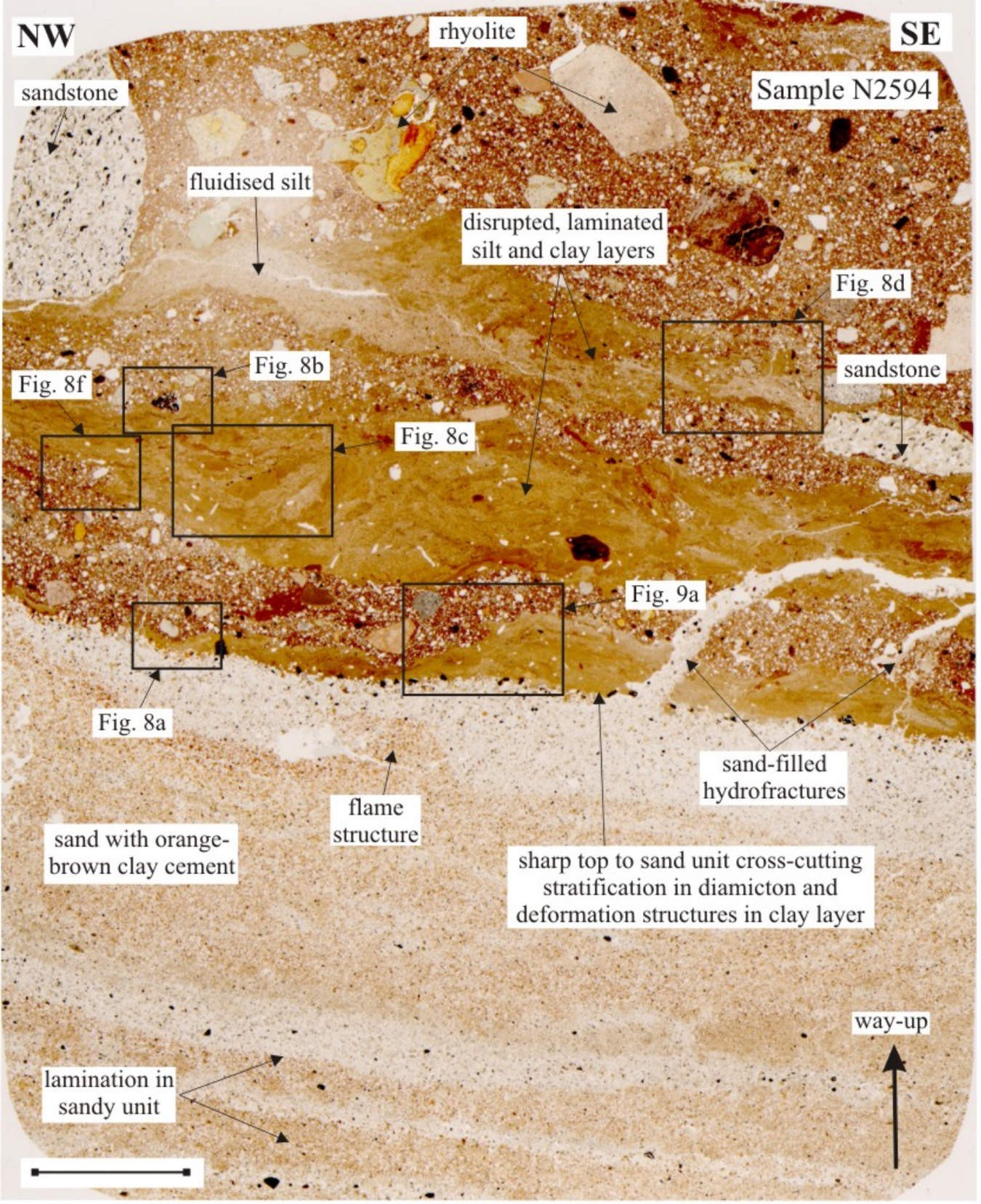

stratified base of diamicton with layering defined by highly deformed clay and silt layers

laminated matrix-poor sand with locally developed cement-supported texture

Figure 7.

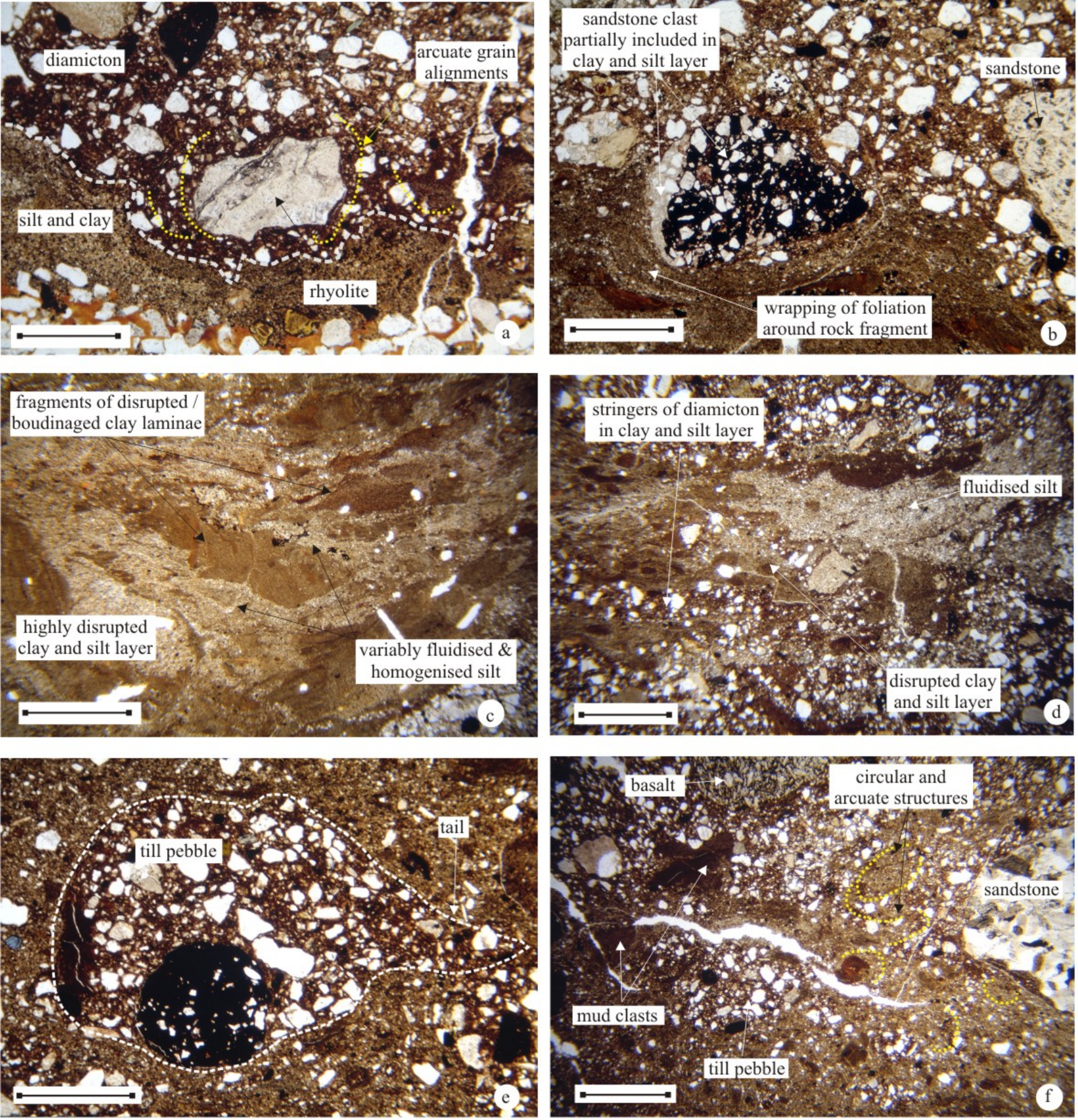
diamicton
arcuate grain alignments
silt and clay
rhyolite
a
sandstone clast partially included in clay and silt layer
sandstone
wrapping of foliation around rock fragment
b
fragments of disrupted / boudinaged clay laminae
highly disrupted clay and silt layer
variably fluidised & homogenised silt
c
stringers of diamicton in clay and silt layer
fluidised silt
disrupted clay and silt layer
d
till pebble
tail
e
basalt
circular and arcuate structures
sandstone
mud clasts
till pebble
f

Figure 8.

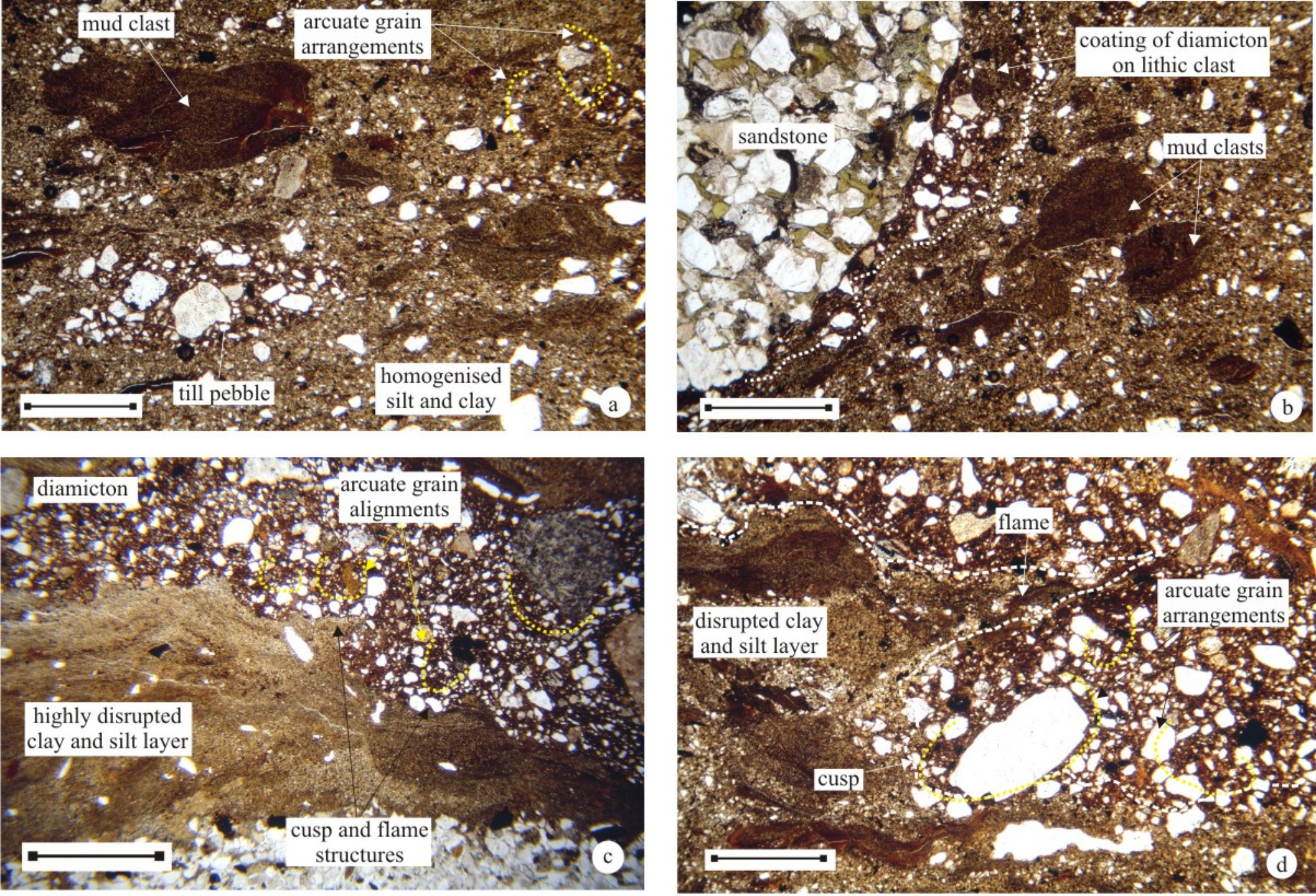
mud clast
arcuate grain arrangements
till pebble
homogenised silt and clay
a
coating of diamicton on lithic clast
sandstone
mud clasts
b
diamicton
arcuate grain alignments
highly disrupted clay and silt layer
cusp and flame structures
c
flame
arcuate grain arrangements
disrupted clay and silt layer
cusp
d

Figure 9.

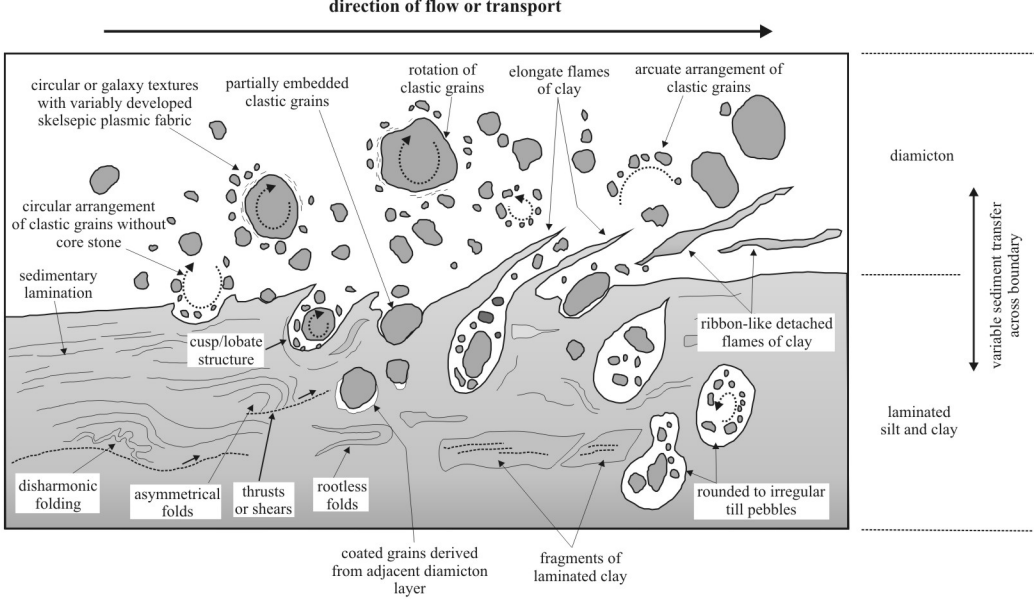
direction of flow or transport
circular or galaxy textures with variably developed skelsepic plasmic fabric
partially embedded clastic grains
rotation of clastic grains
elongate flames of clay
arcuate arrangement of clastic grains
diamicton
circular arrangement of clastic grains without core stone
sedimentary lamination
cusp/lobate structure
ribbon-like detached flames of clay
variable sediment transfer across boundary
laminated silt and clay
disharmonic folding
asymmetrical folds
thrusts or shears
rootless folds
rounded to irregular till pebbles
coated grains derived from adjacent diamicton layer
fragments of laminated clay
Progressive development and detachment of flames and associated cusp/lobate structures resulting in the formation of till pebble and clay ribbons
Increasing internal disruption of laminated clay-silt layer accompanied by fludisation of silt laminae

Figure 10.

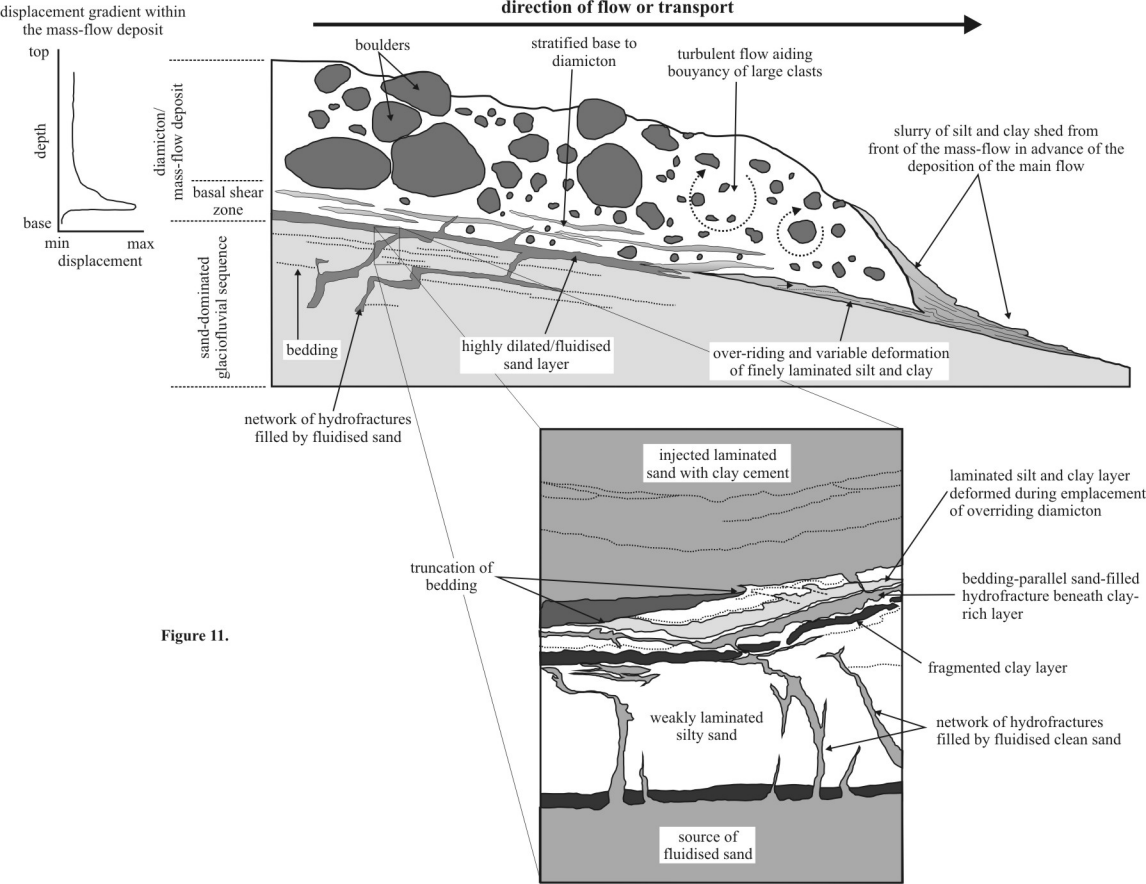
displacement gradient within the mass-flow deposit
top
depth
base
min
max
displacement
direction of flow or transport
diamicton/ mass-flow deposit
basal shear zone
sand-dominated glaciofluvial sequence
boulders
stratified base to diamicton
turbulent flow aiding bouyancy of large clasts
slurry of silt and clay shed from front of the mass-flow in advance of the deposition of the main flow
bedding
highly dilated/fluidised sand layer
over-riding and variable deformation of finely laminated silt and clay
network of hydrofractures filled by fluidised sand
injected laminated sand with clay cement
laminated silt and clay layer deformed during emplacement of overriding diamicton
truncation of bedding
bedding-parallel sand-filled hydrofracture beneath clay-rich layer
fragmented clay layer
weakly laminated silty sand
network of hydrofractures filled by fluidised clean sand
source of fluidised sand

Figure 11.

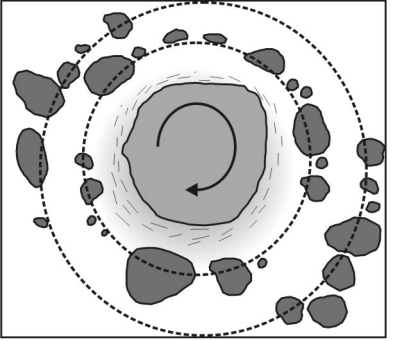

concentric arrangement of grains around larger clast with variably developed skelsepic plasmic fabric and concentration of fines around the margin of the large clast

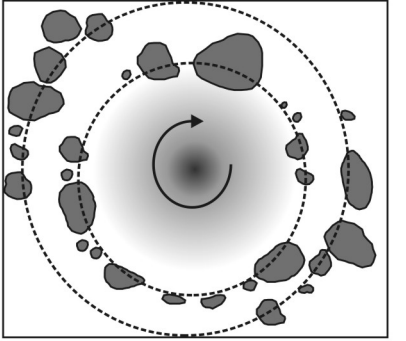

concentric arrangement of grains without a 'corestone', possibly with concentration of fines in the center of the structure

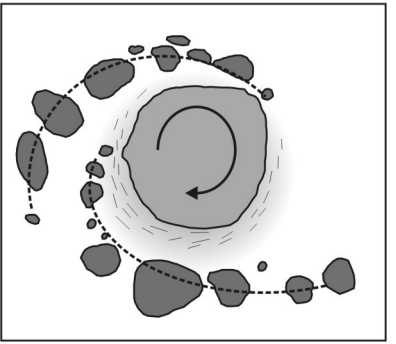

spiral arrangement of grains around larger clast (galaxy structure) with variably developed skelsepic plasmic fabric and concentration of fines around the margin of the large clast

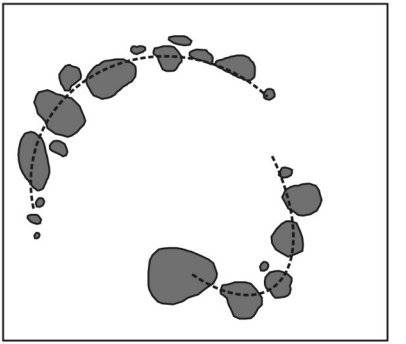

arcuate clusters of grains may be isolated within the matrix of the diamicton or associated with larger clastic grains

Figure 12.

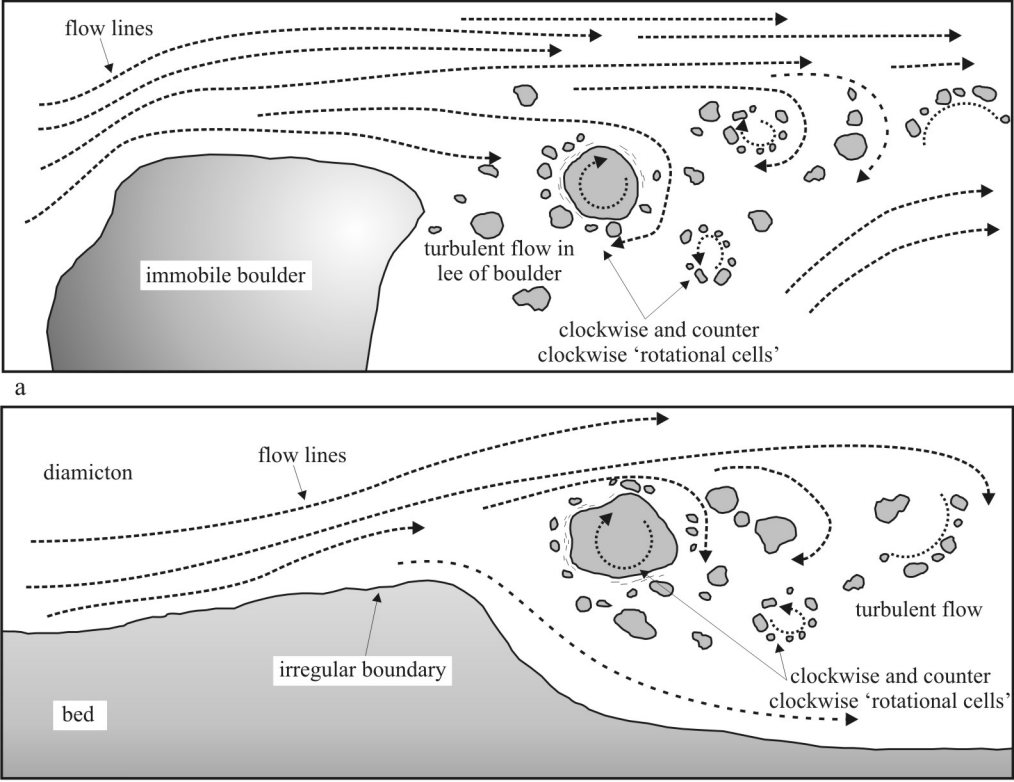
flow lines
immobile boulder
turbulent flow in
lee of boulder
clockwise and counter
clockwise 'rotational cells'
a
diamicton
flow lines
turbulent flow
irregular boundary
clockwise and counter
clockwise 'rotational cells'
bed
b

Figure 13.

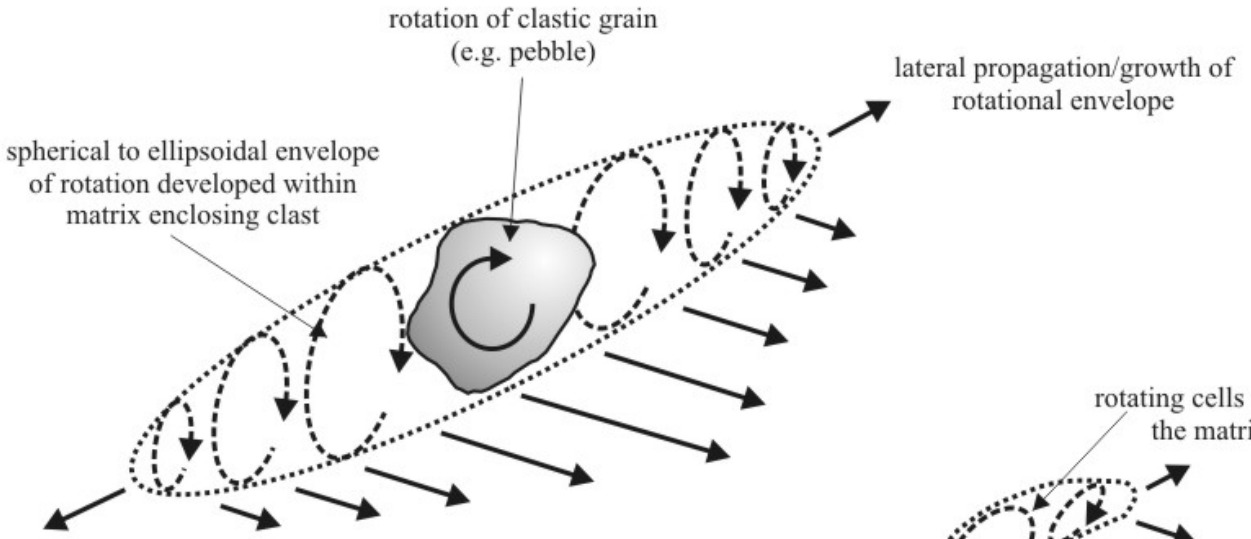

Stage 1. Development and migration of the rotational cell through the matrix of the diamicton

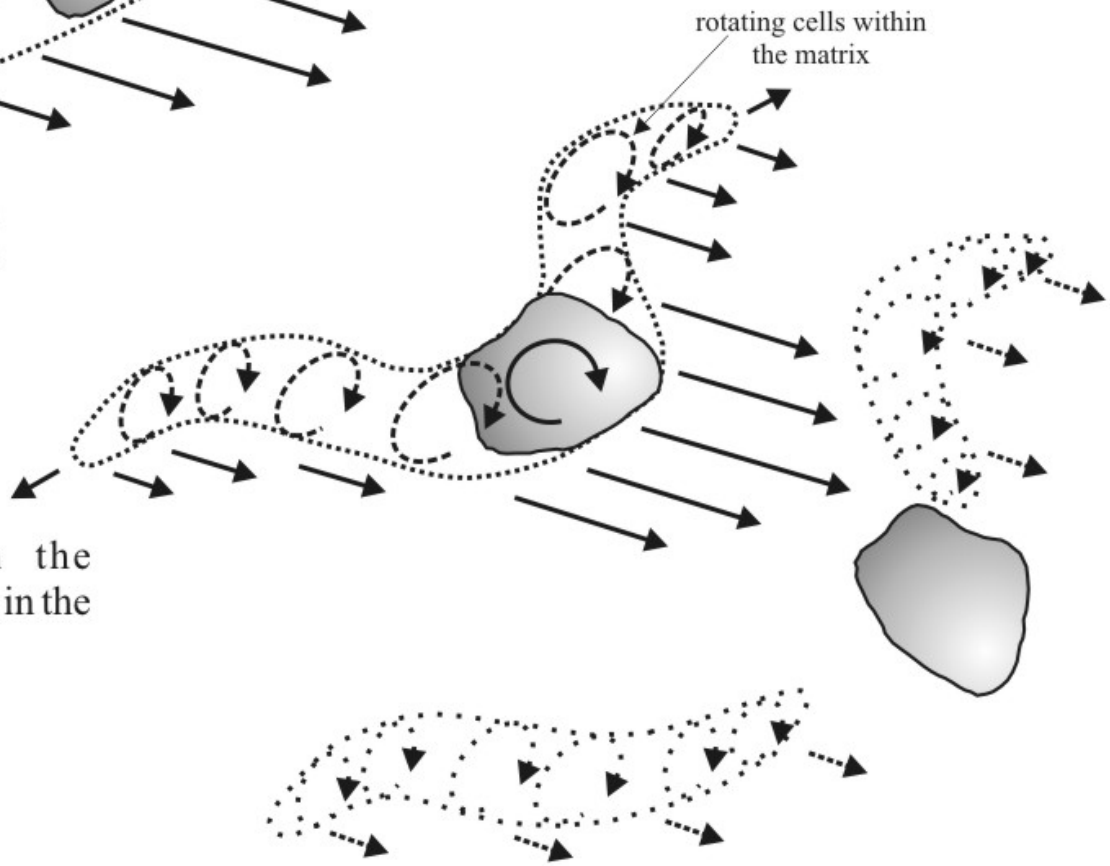

Stage 2. Lateral variation in the velocity/degree of migration resulting in the distortion of the rotational cell

Stage 3. Eventual segmentation and collapse of the rotational cell possibly associated with cessation of clast rotation

Figure 14.